Quantum and Semiclassical Non-Hermitian Dicke Models without Nonreciprocity

Bin Jiang(姜斌)[1], Yi-Yang Li(李依阳)[2], Jun-Jie Liu(刘俊杰)[3,4], Chen Wang(王晨)[5*], and Jian-Hua Jiang(蒋建华)[1,2,6,7*]

[1]*Department of Modern Physics, School of Physical Sciences, University of Science and Technology of China, Hefei 230026, China*
[2]*School of Physical Science and Technology & Collaborative Innovation Center of Suzhou Nano Science and Technology, Soochow University, Suzhou 215006, China*
[3]*Department of Physics, International Center of Quantum and Molecular Structures, Shanghai University, Shanghai 200444, China*
[4]*Institute for Quantum Science and Technology, Shanghai University, Shanghai 200444, China*
[5]*Department of Physics, Zhejiang Normal University, Jinhua 321004, China*
[6]*School of Biomedical Engineering, Division of Life Sciences and Medicine, University of Science and Technology of China, Hefei 230026, China*
[7]*Suzhou Institute for Advanced Research, University of Science and Technology of China, Suzhou 215123, China*

(Received 19 August 2025; accepted manuscript online 17 October 2025)

The Dicke model, which describes the collective interaction between an ensemble of atoms and a single-mode photon field, serves as a fundamental framework for studying light-matter interactions and quantum electrodynamic phenomena. In this work, we investigate the manifestation of non-Hermitian effects in a generalized Dicke model, where two dissipative atom ensembles interact with a single-mode photon field. We explore the system in the semiclassical limit as a non-Hermitian Dicke model, revealing rich exceptional points (EPs) and diabolic points. Furthermore, we explore the quantum signature of EPs in the Hilbert space, relying on discrete photon numbers. The transition of photons from antibunching to bunching at steady state is unravelled. Our findings deepen the understanding of non-Hermitian physics in light-matter interaction, which is instructive for the design of advanced photonic devices.

DOI: 10.1088/0256-307X/42/12/120403 CSTR: 32039.14.0256-307X.42.12.120403

1. Introduction. Non-Hermitian systems are described by non-Hermitian Hamiltonians, of which the eigenvalues are real under parity-time (PT) symmetry, whereas complex eigenvalues occur once such symmetry is broken.[1] Progress in non-Hermitian physics has significantly advanced the understanding of non-equilibrium systems and impacted development in other fields, including quantum information science, materials science, and topological physics.[2–7] An exceptional point (EP) emerges as a spectral singularity where the eigenvalues coincide and the eigenvectors coalesce, giving rise to quantum-enhanced sensing and therefore being important for quantum technology.[8–10]

Non-Hermitian light-matter interacting systems have attracted much attention both in semiclassical[11–13] and quantum regimes.[5,14–17] They generally yield PT-symmetry breaking, including PT-symmetry controlled lasers,[18–20] non-Hermitian skin effects,[21–23] non-Hermitian quantum sensors,[10,24,25] unconventional quantum thermodynamics,[26,27] and non-Hermitian quantum phase transitions.[28] The Dicke model,[29] a prototype model of light-matter-interacting systems, characterizes the collective interaction between an ensemble of atoms and a single-mode photon field, and is known to yield superradiant phase transitions[30] and criticality-enhanced sensing.[8,9] Counter-rotating-wave contributions,[31] anisotropic couplings,[32] and two-photon processes[33] fertilize light-matter interactions on the superradiant phase transition. When non-Hermitian effects are included via nonreciprocal couplings[34,35] or complex potential energy,[36,37] unconventional superradiant phase transition features have been revealed in the Dicke model. However, the implementation of nonreciprocal couplings often requires sophisticated designs, e.g., synthetic gauge fields, which can introduce additional experimental complexity and decoherence channels.

This work explores a distinct pathway to non-Hermitian physics in a generalized Dicke model. Instead of breaking reciprocity, we employ balanced gain and loss between two reciprocally coupled atomic ensembles to achieve PT-symmetry. This approach not only simplifies the experimental requirements by leveraging intrinsic dissipative processes but also, as we will demonstrate, enables the emergence of higher-order EP that are typically challenging to stabilize in nonreciprocal systems due to their heightened parameter sensitivity. Higher-order EPs, i.e., the coalescence of multiple eigenvalues at fine-tuned parameters, are explored.[38–40] So far, most studies have fo-

*Corresponding authors. Email: wangchen@zjnu.cn; jhjiang3@ustc.edu.cn
© 2025 Chinese Physical Society and IOP Publishing Ltd. All rights, including for text and data mining, AI training, and similar technologies, are reserved.

cused mainly on second-order EPs (EP2s) in two-level systems as the simplest prototypes of EPs. With higher-order EPs, a system can be very sensitive to external perturbations and exhibit versatile quantum geometry.[39] Generally to achieve an n-th order EP, one needs $2n-2$ tunable physical parameters,[38] which makes the realization of higher-order EPs rather challenging.

In this letter, we find that the non-Hermitian Dicke Hamiltonian in the semiclassical limit has rich EP formation patterns, e.g., third-order EPs (EP3s). In the quantum limit, i.e., when the number of photons is small, the quantum signature of EPs is analyzed, featuring photon-number-dependent EPs. The influence of non-hermiticity on the photon statistics, e.g., photon bunching and antibunching, is studied. Our findings reveal the nontrivial non-Hermitian physics underlying the non-Hermitian Dicke systems, providing physical insights for the design of non-Hermitian light-matter interacting devices.

2. Non-Hermitian Dicke Models. The generalized Dicke model in Fig. 1(a), which is composed of two coupled atom ensembles interacting with a quantized photon field, reads

$$\hat{H}_{\rm Dicke} = \sum_{j=1,2}\omega_j\hat{J}_j^z + \omega_{\rm p}\hat{a}^\dagger\hat{a} + \frac{t}{\sqrt{N_1N_2}}(\hat{J}_1^+\hat{J}_2^- + \hat{J}_1^-\hat{J}_2^+) + \sum_{j=1,2}\frac{\kappa_j}{\sqrt{2N_j}}(\hat{a}^\dagger\hat{J}_j^- + \text{h.c.}), \quad (1)$$

where $\hat{J}_i^\alpha = \sum_{n=1}^{N_i}\hat{s}_\alpha^n$ $(\alpha = z,+,-)$ describes the collective angular momentum operator consisting of N_i spin-1/2 atoms with the transition energy ω_i, $\hat{a}^\dagger(\hat{a})$ creates(annihilates) one photon with the frequency $\omega_{\rm p}$, κ_i denotes the coupling strength between atomic ensembles and the photon field, and t shows the collective angular momentum coupling strength. Crucially, our model preserves reciprocity of the light-matter interactions, distinct from nonreciprocal counterparts.[34,35] Moreover, such a non-Hermitian Dicke model can be effectively obtained from the microscopic Lindblad equation [see Section I of the Supplementary Materials (SM)]. We consider the influence of non-Hermitian effects on the quantum Dicke model via separate gain and loss processes on atom ensembles, which is described as $\hat{H}_{\rm nDicke} = \hat{H}_{\rm Dicke} + \sum_{j=1,2}\frac{i\gamma_j}{N_j}\hat{J}_j^+\hat{J}_j^-$. The positive (negative) γ_j $(j=1,2)$ denotes the gain (loss) strength of the jth collective angular momentum to break the hermiticity of the Dicke model.

Then we include the Holstein–Primakoff transformation[41] to describe collective angular momentum operators, i.e., $\hat{J}_i^+ = \hat{b}_i^+\sqrt{N_i - \hat{b}_i^+\hat{b}_i}$, $\hat{J}_i^- = \sqrt{N_i - \hat{b}_i^+\hat{b}_i}\,\hat{b}_i$, and $\hat{J}_i^z = \hat{b}_i^+\hat{b}_i - N_i/2$. Considering the weak excitation of collective angular momentum operators $\langle\hat{b}_i^+\hat{b}_i\rangle \ll N_i$, the non-Hermitian Dicke model in the semiclassical limit, as shown in Fig. 1(b), can be reexpressed as

$$\hat{H}_{\rm cDicke} = \sum_{j=1,2}(\omega_j + i\gamma_j)\hat{b}_j^\dagger\hat{b}_j + \omega_0\hat{a}^\dagger\hat{a} + t(\hat{b}_1^\dagger\hat{b}_2 + \hat{b}_1\hat{b}_2^\dagger) + \sum_{j=1,2}\frac{\kappa_j}{\sqrt{2}}(\hat{b}_j^\dagger\hat{a} + \text{h.c.}). \quad (2)$$

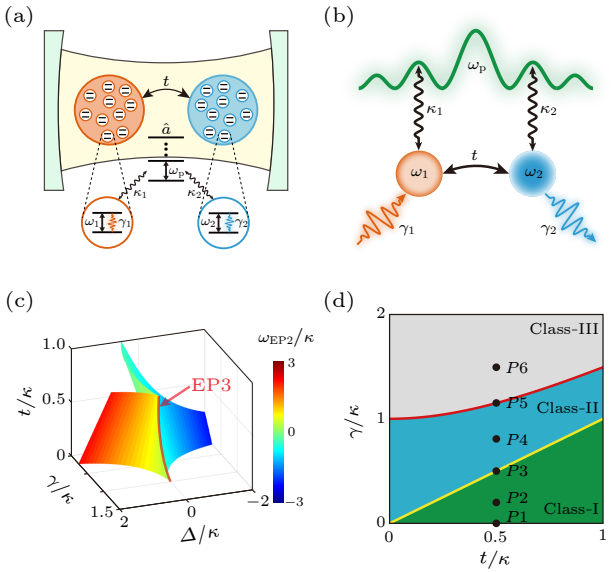

Fig. 1. (a) Schematic of the non-Hermitian quantum Dicke model, where two coupled atom ensembles interact with a quantized photon field. The collective angular momentum operator consisted of N_i spin-1/2 atoms with the transition energy ω_i $(i=1,2)$, while $\hat{a}$ denotes the annihilation operator for a photon with the frequency $\omega_{\rm p}$. κ_i denotes the coupling strength between each atom and the photon field, and t indicates the collective angular momentum coupling strength. Positive (negative) γ_i denotes the gain (loss) strength of the ith collective angular momentum. (b) Schematic of the non-Hermitian Dicke model in the semiclassical regime, where two coupled atom (depicted as orange and blue solid circles) ensembles interact with a single-mode photonic field (green wavy line). (c) The second/third-order EPs (EP2s/EP3s) in 3D parameter spaces $\{\Delta/\kappa, \gamma/\kappa, t/\kappa\}$. The intersection of two EP2 surface branches (half-transparent red line) outlines the trajectory of EP3. (d) The EP phase diagram of the semiclassic Dicke model in 2D parameter spaces $\{\gamma/\kappa, t/\kappa\}$. The green, blue, and gray regions represent classes I, II, and III exceptional points formation patterns (EPFPs), respectively. The solid red curve marks the formation of EP3, while the solid yellow line indicates the transition of EP2. The six black dots, labeled from $P1$ to $P6$, along a vertical line, represent specific EPFPs, as illustrated in Fig. 2. In panels (c) and (d), $\Delta = \omega_{\rm a} - \omega_{\rm p}$ represents the frequency detuning between the atom ensemble and the photon field under the assumption of two identical atom ensembles, i.e., $\omega_{1(2)} = \omega_{\rm a}$ and $\kappa_{1(2)} = \kappa$.

3. High-Order EPs. We investigate high-order EPs in a non-Hermitian semiclassical three-mode Dicke model. The emergence of multiple EPs and their interactions are summarized in a phase diagram, each region owing unique EP formation patterns (EPFPs).[42] Furthermore, we assess the order of singularities of EPs employing the concept of phase rigidity, confirming EP3 (EP2) as a third (second) order singularity.

Here we specifically consider two identical atom ensembles, i.e., $\omega_{1(2)} = \omega_{\rm a}$ and $\kappa_{1(2)} = \kappa$. We note that EP3 requires effective gain and loss, e.g., $\gamma_1 = -\gamma_2 = \gamma$; passive loss alone does not suffice (see Section II of the SM). We reexpress the semiclassical Dicke model as $\hat{H}_{\rm cDicke} = [\hat{b}_1^\dagger, \hat{a}^\dagger, \hat{b}_2^\dagger](\omega_{\rm p}\hat{I}_{3\times3} + \mathcal{H})[\hat{b}_1, \hat{a}, \hat{b}_2]^{\rm T}$, where the corresponding

Dicke matrix is specified as

$$\mathcal{H} = \begin{bmatrix} \Delta + \mathrm{i}\gamma & \kappa/\sqrt{2} & t \\ \kappa/\sqrt{2} & 0 & \kappa/\sqrt{2} \\ t & \kappa/\sqrt{2} & \Delta - \mathrm{i}\gamma \end{bmatrix} \tag{3}$$

with $\Delta = \omega_\mathrm{a} - \omega_\mathrm{p}$ the frequency detuning between the atom ensemble and the photon field. In the following analysis, κ is set as the energy unit.

We include Eq. (3) to investigate EPs in Fig. 1(c) by tuning dimensionless parameters t/κ, γ/κ, and Δ/κ. The emergence of EP2 indicates that the eigenvalue spectra include two conjunctive eigenvalues ω_{EP2} and another single eigenvalue ω_3. The application of Vieta's formulas yields the EP2 condition (Eq. S14 in SM). Figure 1(c) shows two EP2 surface branches, whose intersection (semi-transparent red line) defines the EP3 trajectory. Under such a search bound $\omega_{\mathrm{EP2}} = \omega_3 = \omega_{\mathrm{EP3}}$, Eq. S14 of the SM can be reduced to $\Delta = \frac{3}{2}\omega_{\mathrm{EP3}}$, $\gamma = (\omega_{\mathrm{EP3}}^2 + \kappa^2)^{\frac{3}{2}}/\kappa^2$, and $t = \frac{3}{2}\omega_{\mathrm{EP3}} + \frac{\omega_{\mathrm{EP3}}^3}{\kappa^2}$. Therefore, the signal of high-order EPs can be explicitly observed by tuning the system parameters.

Then we study eigenvalues in Eq. (3) as a function of Δ/κ and analyze the distribution of EPs by tuning t/κ and γ/κ. Figure 1(c) shows that depending on the parameters t/κ and γ/κ, different combinations of EP2 and EP3 consist of different EPFPs. Figure 1(d) shows a bird's-eye view of the EP phase diagram. Specifically, there are three distinct regions marked as class I, II, and III, with their boundaries highlighted by a solid yellow line and a solid red line. Each region has unique EPFPs.

To present the EPFP in each region, the intersite coupling is given a special value of $t/\kappa = 0.5$, and then we gradually increase γ/κ from 0 (point $P1$) to 1.5 (point $P6$), as marked by black points in Fig. 1(d). The point $P1$ ($\gamma/\kappa = 0$) obtained by tuning off the balance loss and gain is a Hermitian case, whose spectrum is shown in Fig. 2(a). There is a linear crossing diabolic point (DP) at $\Delta/\kappa = t/\kappa$. We stress that such a linear crossing DP in the Hermitian system is essentially different from EPs in non-Hermitian systems, where the singularity (the coalescence of multiple eigenstates simultaneously) is found.

Once we slightly break hermiticity in our Dicke model by introducing a finite balance gain and loss, e.g., $\gamma/\kappa = 0.2$, the linear crossing DP in the Hermitian system will split into two EP2s with opposite chirality, which gives a typical EPFP of class-I (point $P2$), as shown in Fig. 2(b). Here, we define the chirality of EPs according to their eigenstates. Generally for an N-state system described by $\hat{H}(\boldsymbol{\lambda})$, the eigenvector $|\psi_{\mathrm{EP2}}\rangle$ at a EP2 admits[43]

$$|\psi_{\mathrm{EP2}}^{\mathrm{R}}\rangle = \sum_k c_k(\boldsymbol{\lambda})|\chi_k^{\mathrm{R}}(\boldsymbol{\lambda})\rangle, \quad \boldsymbol{\lambda} \to \boldsymbol{\lambda}_{\mathrm{EP2}}, \tag{4}$$

where coefficients are given by $c_k(\boldsymbol{\lambda}) = \langle\chi_k^{\mathrm{L}}|\psi_{\mathrm{EP2}}\rangle$ and superscript "R" and "L" refer to the right and left eigenvectors, respectively. As the parameter vector $\boldsymbol{\lambda}$ approaches EP $\boldsymbol{\lambda}_{\mathrm{EP2}}$, the two coalescing eigenvectors $|\chi_1^{\mathrm{R}}(\boldsymbol{\lambda})\rangle$ and $|\chi_2^{\mathrm{R}}(\boldsymbol{\lambda})\rangle$ diverge, while the remaining $N-2$ eigenvectors $|\chi_k^{\mathrm{R}}(\boldsymbol{\lambda})\rangle$ remain regular.

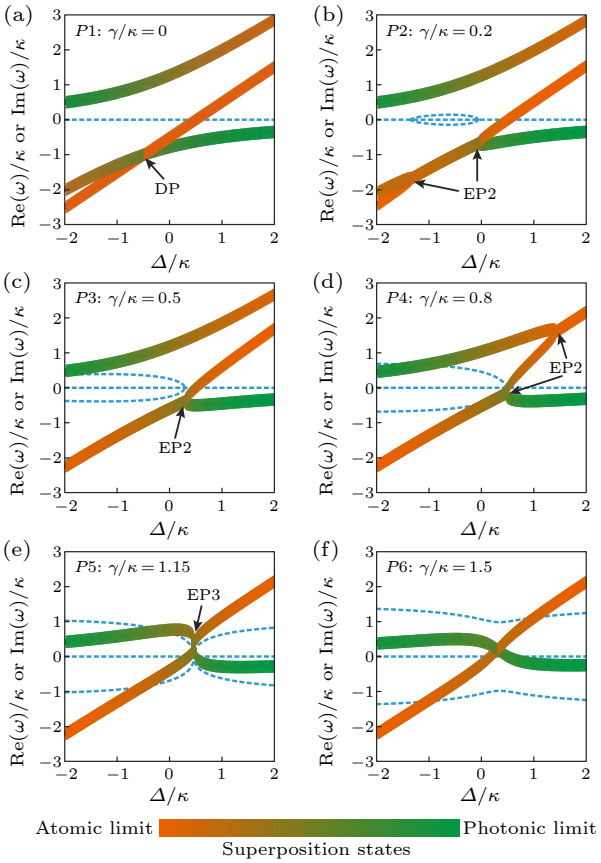

Fig. 2. Eigenvalues as a function of frequency detuning Δ/κ from points $P1$ to $P6$ within the phase diagram in Fig. 1(d), accordingly. The solid lines represent the real part of the eigenvalues, while the dashed lines represent the imaginary part. The real part of the frequency eigenvalues is colored according to the eigenstates, as labeled by the colorbar at the bottom of the figure: The red (green) color stands for the states in atomic (photonic) limit, while a superposition state is represented by the color in between. Here, the states in photoinc (atomic) limit means you will find a photon (or an atom, either the first one or the second one) at an one hundreds present probability if you detect the eigenstates, otherwise the states are called superposition states. Thus, the color change represents the change in probability amplitudes of the eigenstates. All parameters are normalized by κ and $t/\kappa = 0.5$ is adopted for all panels. The balanced gain (loss) strength γ/κ is given in the top left corner of each panel. Each exceptional or degenerate point is labeled to show its type according to the main text except panel (f), the PT-broken phase without EP.

Consequently, near the EP, the expansion (4) is dominated by the terms corresponding to $k = 1, 2$. Moreover, due to the biorthogonality of left and right eigenvectors from distinct states, all coefficients c_k for $k \neq 1, 2$ approach zero. Thus, in the limit $\boldsymbol{\lambda} \to \boldsymbol{\lambda}_{\mathrm{EP2}}$ the N-dimensional vector $|\psi_{\mathrm{EP2}}^{\mathrm{R}}\rangle$ reduces to a superposition of the two N-dimensional vectors $|\chi_1^{\mathrm{R}}(\boldsymbol{\lambda})\rangle$ and $|\chi_2^{\mathrm{R}}(\boldsymbol{\lambda})\rangle$. Based on analysis of the two-state model,[44] it is anticipated that near $\boldsymbol{\lambda}_{\mathrm{EP2}}$ the coefficient ratio satisfies $c_1/c_2 = +\mathrm{i}$ or $c_1/c_2 = -\mathrm{i}$.

In the process of continuously increasing γ/κ, it is found that the occurring positions of two EP2 are in opposite directions, and the left one disappears (or moves to

negative infinite far from another EP2) when $\gamma/\kappa = t/\kappa = 0.5$, as shown in Fig. 2(c). The value of $\omega_{\rm EP2}$ is greater than ω_3 only if t/γ is less than 1. Therefore, the yellow curve $t/\gamma = 1$ in Fig. 1(d) is a critical middle phase during the process of increasing γ/t. The yellow line $\gamma = t$ in Fig. 1(d) separates class I from class II, marking the transition of an EP2 from the lower energy gap to the higher one. This phase boundary is of particular importance because it not only shifts the location of the EP2 but also flips its chirality. Below the yellow line in the region of class I, two EP2 appear in the same energy gap with opposite chirality, while above the yellow line in the region of class II, two EP2 with the same chirality appear in adjacent energy gaps and their corresponding EPFP are shown in Fig. 2(d). Upon a further increase in γ/κ, the system will meet with red line in Fig. 1(d). As shown in Fig. 2(e), the configuration of point $P5$ on the red line always exists a EP3 at a particular value of Δ/κ. Moreover, we note that further increasing γ/κ brings the Dicke model into region class III, where the system will thoroughly lose PT symmetry and the real part of the eigenvalue of EP3 still keeps degenerating, while the imaginary parts are expected to splitting [point $P6$ in Fig. 1(d) and its corresponding eigenvalues spectra in Fig. 2(f)].

Before delving into the singularities of EPs, it is worth summarizing the rules that govern the coalescence of two or more EPs. The emergence of an EP3 can be understood as the merging of two EP2s in adjacent energy gaps with the same chirality. In contrast, when EP2s with the same energy gap and chirality collide, they merge into a linear crossing EP2, a phenomenon also found in Ref. [42]. A linear crossing DP in Hermitian systems forms through the merger of two EP2s within the same energy gap but with opposite chirality, which can be observed during the reversal detuning process from $P2$ to $P1$. It is important to note that the linear crossing EP2 in non-Hermitian systems is distinct from the linear crossing DP in Hermitian systems, as the latter does not exhibit any spectral singularity. We also investigate the critical behaviors of EPs in Fig. 1(d), directly confirming that the red (yellow) line is indeed a high-order EP3 (EP2) singularity line (see Section III of the SM). Extensions to nonlinear gain and a 1D Dicke chain reveal even richer phenomena, including higher-order nonlinear EPs, non-Hermitian dynamics and non-Hermitian topological states (see Sections IV–VI of the SM).

Moreover, we note that this non-Hermitian matrix in Eq. (3) could be considered as the description of non-Hermiticity in the second-quantized basis. If one goes back to the first-quantized picture in the Fock states, analogous EP signatures can also be observed, which will be demonstrated in the following section.

4. Quantum Signature of EPs. We investigate EPs in the quantum regime of the Dicke model by applying the Lindblad master equation[45] [also see Section I Eq. (S2) of the SM]. When we only include the trajectories without quantum jumps, the effective non-Hermitian Dicke Hamiltonian denotes $\hat{H}_{\rm eff} = \hat{H}_{\rm Dicke} + {\rm i}\sum_j \gamma_j/N_j \hat{J}_j^+ \hat{J}_j^-$. In particular, the single qubit case (i.e., $N_j = 1$) is the generic quantum light-matter interacting model (i.e., Jaynes–Cummings model). We should admit that it is rather difficult to analytically obtain EPs with small photon excitation even at $N_j = 1$. While at large n regime under the basis $\{|\uparrow\uparrow n\rangle, |\uparrow\downarrow n+1\rangle, |\downarrow\uparrow n+1\rangle, |\downarrow\downarrow n+2\rangle\}$, the non-Hermitian Hamiltonian can be approximately simplified as $\hat{H}_{\rm eff} \approx [\omega_{\rm p}(n+1) - {\rm i}\frac{\Gamma}{2}]\boldsymbol{I}_{4\times4} + \mathcal{H}$, where the kernel component denotes

$$\mathcal{H} = \begin{bmatrix} \delta - {\rm i}\Gamma & \kappa\sqrt{n}/\sqrt{2} & \kappa\sqrt{n}/\sqrt{2} & 0 \\ \kappa\sqrt{n}/\sqrt{2} & {\rm i}\gamma & t & \kappa\sqrt{n}/\sqrt{2} \\ \kappa\sqrt{n}/\sqrt{2} & t & -{\rm i}\gamma & \kappa\sqrt{n}/\sqrt{2} \\ 0 & \kappa\sqrt{n}/\sqrt{2} & \kappa\sqrt{n}/\sqrt{2} & -\delta + {\rm i}\Gamma \end{bmatrix} \tag{5}$$

with $\delta = \omega_{\rm a} - \omega_{\rm p}$, $\Gamma = (\gamma_2 + \gamma_1)/2$, and $\gamma = (\gamma_2 - \gamma_1)/2$. If we further consider the absence of atom–atom coupling $t = 0$ and the asymmetric dissipation condition of two atoms $\gamma_2 \ll \gamma_1$, which leads to $\gamma = -\Gamma$, the positions of EP2 under $\delta = 0$ can be determined at

$$\Gamma = \pm\kappa\sqrt{n}/\sqrt{2} \tag{6}$$

with the expression of $E_{\pm,n}^2 = -(\Gamma^2 - n\kappa^2) \pm \sqrt{(\Gamma^2 - n\kappa^2)^2 - \Gamma^4}$ and $n \geq 0$. We note that the EPs are obtained in the Hilbert space, which highly depend on the quantized photon number n. This is the signature of the quantum effect.[48] In contrast, the EPs in the semiclassical Dicke model were calculated with the bosonic modes, rather than in the Hilbert space.

Now we consider the single excitation case of the quantum Dicke model. Under the basis $\{|\uparrow\downarrow 0\rangle, |\downarrow\uparrow 0\rangle, |\downarrow\downarrow 1\rangle\}$, the reduced effective Hamiltonian is described as $\hat{H}_{\rm eff} = \omega_0 \boldsymbol{I}_{3\times3} + \mathcal{H}'$, where $\mathcal{H}'$ denotes submatrix of $\mathcal{H}$ at Eq. (5) with $n = 1$ and $\Gamma = 0$, by eliminating the first row and column. Moreover, if we set $\delta = 0$, the effective Hamiltonian matrix $\mathcal{H}'$ is reduced to Eq. (3). Hence the EP2 solution is generally expected to be observed, for the kernel Hamiltonian component is analogous with the non-Hermitian semiclassical Dicke model in the absence of atom gain. In particular, once we set $\gamma_2 = -\gamma_1 = \gamma$, EP3 can also be detected. However, these are quantum signatures of EPs in Hilbert space.

5. Photon Statistics. The nonclassicality of photons is widely regarded as a crucial topic in the quantum community, attracting persistent attention in quantum optics and quantum information processing. The two-photon correlation function is considered as one of the main characteristics initially proposed by R. J. Glauber in the quantum theory of optical coherence. Consequently, a two-photon correlation function has been extensively used in various quantum light–matter interaction systems, including dissipative quantum Rabi and finite-size Dicke models. The steady-state two-photon correlation function with no time delay is defined as

$$G_{\rm ss}^{(2)}(\tau) = \frac{\langle \hat{a}^\dagger \hat{a}^\dagger(\tau)\hat{a}(\tau)\hat{a}\rangle_{\rm ss}}{\langle \hat{a}^\dagger \hat{a}\rangle_{\rm ss}^2}, \tag{7}$$

where $\langle \hat{O}\rangle_{\rm ss} = {\rm Tr}\{\hat{O}\hat{\rho}_{\rm ss}\}$, with $\hat{\rho}_{\rm ss}$ the steady state of the quantum system.

We investigate the influence of PT symmetry on two-photon statistics. It is known that the steady state at dynamical Eq. (5) is the trivial ground state of $\hat{D}_{\rm Dicke}$, i.e., $\hat{\rho}_{\rm s} = |{\downarrow\downarrow}\,0\rangle\langle{\downarrow\downarrow}\,0|$. Thus, to efficiently observe the nonclassical photon correlation, we include a weak driving field to excite photons, leading to the system Hamiltonian $\hat{H}_{\rm t-Dicke} = \hat{H}_{\rm Dicke} + \eta(e^{i\omega_{\rm d}t}\hat{a} + e^{-i\omega_{\rm d}t}\hat{a}^\dagger)$, with η and $\omega_{\rm d}$ being the driving amplitude and frequency, respectively. Under the rotating framework, i.e., the rotated Hamiltonian becomes $\hat{H}_{\rm R} = \sum_{j=1,2}\Delta_j\hat{J}_j^z + \Delta_{\rm p}\hat{a}^\dagger\hat{a} + \frac{t}{\sqrt{N_1N_2}}(\hat{J}_1^+\hat{J}_2^- + \hat{J}_1^-\hat{J}_2^+) + \sum_{j=1,2}\frac{\kappa_j}{\sqrt{2N_j}}(\hat{a}^\dagger\hat{J}_j^- + {\rm h.c.}) + \eta(\hat{a} + \hat{a}^\dagger)$, where the detuning frequencies denote $\Delta_j = \omega_j - \omega_{\rm d}$ and $\Delta_{\rm p} = \omega_{\rm p} - \omega_{\rm d}$. Consequently, the Lindblad master equation after the rotating transformation becomes $\frac{\rm d}{{\rm d}t}\hat{\rho}_{\rm s} = -{\rm i}[\hat{H}_{\rm R}, \hat{\rho}_{\rm s}] + \sum_j \gamma_j/N_j(2\hat{J}_j^-\hat{\rho}_{\rm s}\hat{J}_j^+ - \hat{J}_j^+\hat{J}_j^-\hat{\rho}_{\rm s} - \hat{\rho}_{\rm s}\hat{J}_j^+\hat{J}_j^-)$.

Furthermore, we turn to the steady-state two-photon correlation function with weak coherent photon driving (e.g., $\eta = 0.01\gamma$ in Fig. 3). Under weak system-reservoir interactions, it is found that the steady-state solution can be approximately obtained by the dynamical equation $\frac{\rm d}{{\rm d}t}\hat{\rho}_{\rm s} \approx -{\rm i}[\hat{H}_{\rm NH}, \hat{\rho}_{\rm s}]$ with $\hat{H}_{\rm NH} = \hat{H}_{\rm R} + {\rm i}\sum_j \gamma_j/N_j\hat{J}_j^+\hat{J}_j^-$, which is also numerically confirmed. This leads to the steady state $\hat{\rho}_{\rm ss} \approx |\psi_{\rm ss}\rangle\langle\phi_{\rm ss}|$, where $|\psi_{\rm ss}\rangle$ ($|\phi_{\rm ss}\rangle$) is the right (left) eigenvector of $\hat{H}_{\rm NH}$ with the corresponding eigenvalue owning the minimal imaginary component.

Figure 3(a) exhibits the steady-state correlation function with no time delay, based on the non-Hermitian dynamical equation. Near the resonant regime (i.e., $\Delta \approx 0$) the antibunching-to-bunching transition is clearly shown with the increase of qubit–photon coupling strength κ. Such a nonclassical transition of photons is dramatically suppressed as the energy bias increases.

Then, we analyze two components of the two-photon correlation function, i.e., one-photon and two-photon terms in Fig. 3(b), both showing a monotonic decrease by enhancing the coupling strength κ before $\kappa \lesssim 0.5\gamma$. However, the two-photon term $\langle(\hat{a}^\dagger)^2(\hat{a})^2\rangle_{\rm ss}$ shows comparative enhancement by further increasing κ. Furthermore, based on the condition of weak photon excitations and local population distributions in Fig. 3(c), one-photon and two-photon correlation terms can be approximately expressed as $\langle\hat{a}^\dagger\hat{a}\rangle_{\rm ss} \approx (P_{\downarrow,\downarrow,1} + 2P_{\downarrow,\downarrow,2})$ and $\langle(\hat{a}^\dagger)^2(\hat{a})^2\rangle_{\rm ss} \approx 2P_{\downarrow,\downarrow,2}$ with the population $P_{\sigma_1,\sigma_2,n} = \langle\sigma_1,\sigma_2,n|\hat{\rho}_{\rm ss}|\sigma_1,\sigma_2,n\rangle$ under the local basis $\{|\sigma_1,\sigma_2,n\rangle\}$. Hence, the two-photon correlation function can be approximately expressed as $G^{(2)}(0) \approx 2P_{\downarrow,\downarrow,2}/(P_{\downarrow,\downarrow,1})^2$. It is found that tuning up κ leads to the sharp decrease of $P_{\downarrow,\downarrow,2}$ and antibunching behavior of photons. While by further enhancing κ, the additional transition $|\psi_{\uparrow,\downarrow,1}\rangle \to |\psi_{\downarrow,\downarrow,2}\rangle$ under the contribution of $\hat{a}^\dagger\hat{J}_1^-$ will enhance $P_{\downarrow,\downarrow,2}$, which finally lifts up $G^{(2)}(0)$. Therefore, κ is crucial in realizing the antibunching-to-bunching nonclassical transition of photons.

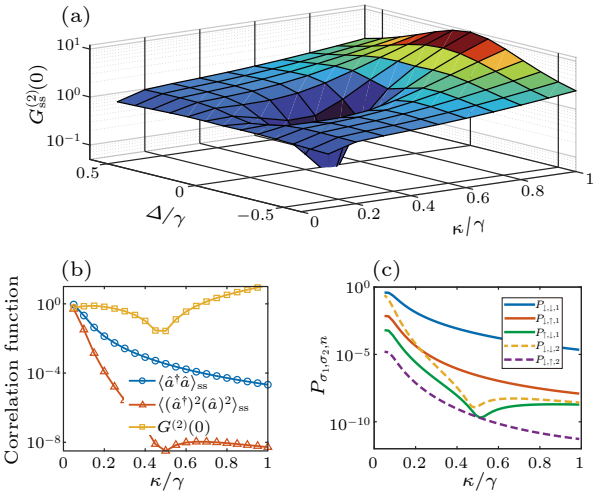

Fig. 3. (a) Zero-time-delay correlation function $G^{(2)}_{\rm ss}(0)$ at steady state by tuning energy bias Δ and qubit–photon coupling strength κ. (b) The correlation function components and (c) local steady-state populations $P_{\sigma_1,\sigma_2,n}$ with $\sigma_j = \uparrow,\downarrow$ and $n = 1, 2$, at $\Delta = 0$. Other system parameters are given by $t = 0$, $\gamma_1 = 1$, $\gamma_2 = 0.3$, and $\eta = 0.01$.

6. Relevant Physical Systems. The Dicke model has been experimentally realized in different setups. The semiclassical Dicke model can be mapped into a model consisting of three interacting resonator modes with different dissipation.[39] This classical regime can be realized in optics (acoustics) where all three resonators are photonic (acoustic) modes. There are several ways to tune the frequency and loss (gain) of each resonator in photonics. One option is to use the thermo-optical effect.[49] Gain and loss can be controlled by, e.g., doping rare-earth elements as the gain medium or tuning the dissipation. In acoustics, the gain can be realized through electrically assisted thermoacoustic generation of sound, as shown in Ref. [50]. The detuning and the couplings between the resonators can be well controlled by the geometry of the acoustic structures (both the resonators and their connections). The second-order and third-order EPs in our model can then be achieved by controlling the detuning and the couplings in these setups.

For the non-Hermitian Dicke model in the quantum regime, it may be established in a setup where two cavities are connected via a fine optical fiber,[51,52] each containing trapped ions, i.e., qubits.[53,54] The hybrid system of two cavities interacting with the common fiber has one dominant mode close to the qubit transition frequency,[55] while other modes can be ignored. Moreover, an external field together with the dominant photon mode drives a Raman transition between two low-energy states of ions. Therefore, we obtain the Dicke model. Additionally, we consider the unbalanced sources of dissipation as spontaneous emission of ions, which leads to Eq. (5).

7. Conclusion and Outlook. In this work, we propose a generalized Dicke model and study the non-Hermitian effects of such a model. In the semiclassical limit, we un-

cover the emergence of higher-order EPs, which substantially affect the system's behavior and enhance its sensitivity to external perturbations. By incorporating nonlinear saturation gain, higher-order nonlinear EPs can emerge at certain parameters where the non-Hermitian eigenstates regain completeness in the temporal dynamics. Moreover, rich topological phase transitions are found where the non-Hermitian effects play an important role. Non-Hermitian semimetal phases are identified where the EPs are extended to exceptional lines.

For the quantum non-Hermitian Dicke model, we investigate the quantum characteristics of the EPs as well as the transition between photon anti-bunching behavior and photon bunching behavior in the steady states, which can be effectively described by the non-Hermitian dynamics. The simplicity of our non-Hermitian Dicke model allows for its implementation in various light–matter interaction systems.

Non-Hermitian Hamiltonians under the post-selection processes generally correspond to the semiclassical limit of open quantum systems. In the quantum regime, in contrast, theoretical descriptions of open quantum systems are usually based on quantum master equations, the path-integral approach,[56] and the non-equilibrium Green's function method.[57,58] Nevertheless, non-Hermitian Hamiltonians provide significant insight into the underlying physics, demonstrating their value in predicting novel phenomena of non-equilibrium systems. Our models and analysis here serve as an example for unraveling both quantum and semiclassical regimes of non-Hermitian physics.

Acknowledgments. This work was supported by the National Key R&D Program of China (Grant No. 2022YFA1404400), the National Natural Science Foundation of China (Grant Nos. 12125504 and 12305050), Zhejiang Provincial Natural Science Foundation (Grant No. LZ25A050001), the Doctoral Support Program for Young Talents of the China Association for Science and Technology, the Hundred Talents Program of the Chinese Academy of Sciences, and the Natural Science Foundation of Jiangsu Higher Education Institutions of China (Grant No. 23KJB140017).

References

[1] Ding K, Fang C, and Ma G 2022 *Nat. Rev. Phys.* **4** 745
[2] Zhu W, Deng W, Liu Y, Lu J, Wang H X, Lin Z K, Huang X, Jiang J H, and Liu Z 2023 *Rep. Prog. Phys.* **86** 106501
[3] Lin R, Tai T, Li L, and Lee C H 2023 *Front. Phys.* **18** 53605
[4] Bergholtz E J, Budich J C, and Kunst F K 2021 *Rev. Mod. Phys.* **93** 015005
[5] Ashida Y, Gong Z, and Ueda M 2020 *Adv. Phys.* **69** 249
[6] Okuma N and Saito M 2023 *Ann. Rev. Cond. Matt. Phys.* **14** 83
[7] Borgnia D S, Kruchkov A J, and Slager R J 2020 *Phys. Rev. Lett.* **124** 056802
[8] Chu Y M, Zhang S L, Yu B Y, and Cai J M 2021 *Phys. Rev. Lett.* **126** 010502
[9] Ilias T, Yang D Y, Huelga S F, and Plenio M B 2022 *PRX Quantum* **3** 010354
[10] Franke J, Muleady S R, Kaubruegger R, Kranzl F, Blatt R, Rey A M, Joshi M K, and Roos C F 2023 *Nature* **621** 740
[11] Wang C, Fu Z, Mao W, Qie J, Stone A D, and Yang L 2023 *Adv. Opt. Photon.* **15** 442
[12] Meng H, Ang Y S, and Lee C H 2024 *Appl. Phys. Lett.* **124** 060502
[13] El-Ganainy R, Khajavikhan M, Christodoulides D N, and Ozdemir S K 2019 *Commun. Phys.* **2** 37
[14] Zhang Z, Zhang Y, Sheng J, Yang L, Miri M A, Christodoulides D N, He B, Zhang Y, and Xiao M 2016 *Phys. Rev. Lett.* **117** 123601
[15] Lodahl P, Mahmoodian S, Stobbe S, Rauschenbeutel A, Schneeweiss P, Volz J, Pichler H, and Zoller P 2017 *Nature* **541** 473
[16] Bernier N R, T'oth L D, Koottandavida A, Ioannou M A, Malz D, Nunnenkamp A, Feofanov A K, and Kippenberg T J 2017 *Nat. Commun.* **8** 604
[17] Sun Y, Shi T, Liu Z, Zhang Z, Xiao L, Jia S, and Hu Y 2023 *Phys. Rev. X* **13** 031009
[18] Yu D and Vollmer F 2021 *Commun. Phys.* **4** 77
[19] Geva A, Sagie G, Gershenzon I, Friesem A, Davidson N, and Raz O 2022 *Sci. Adv.* **8** eabm7454
[20] Zhang Q, Yang C, Sheng J, and Wu H 2022 *PNAS* **119** e2207543119
[21] Liang Q, Xie D, Dong Z, Li H, Li H, Gadway B, Yi W, and Yan B 2022 *Phys. Rev. Lett.* **129** 070401
[22] Zhang X, Zhang T, Lu M H, and Chen Y F 2022 *Adv. Phys. X* **7** 2109431
[23] Li Z, Wang L W, Wang X, Lin Z K, Ma G, and Jiang J H 2024 *Nat. Commun.* **15** 6544
[24] Budich J C and Bergholtz E J 2020 *Phys. Rev. Lett.* **125** 180403
[25] Wiersig J 2020 *Photon. Res.* **8** 1457
[26] Zhang J W, Zhang J Q, Ding G Y, Li J C, Bu J T, Wang B, Yan L L, Su S L, Chen L, Nori F, Özdemir Ş K, Zhou F, Jing H, and Feng M 2022 *Nat. Commun.* **13** 6225
[27] Bu J T, Zhang J Q, Ding G Y, Li J C, Zhang J W, Wang B, Ding W Q, Yuan W F, Chen L, Özdemir Ş K, Zhou F, Jing H, and Feng M 2023 *Phys. Rev. Lett.* **130** 110402
[28] Hanai R, Edelman A, Ohashi Y, and Littlewood P B 2019 *Phys. Rev. Lett.* **122** 185301
[29] Dicke R H 1954 *Phys. Rev.* **93** 99
[30] Kirton P, Roses M M, Keeling J, and Dalla Torre E G 2019 *Adv. Quantum Technol.* **2** 1800043
[31] Lambert N, Emary C, and Brandes T 2004 *Phys. Rev. Lett.* **92** 073602
[32] Das P, Bhakuni D S, and Sharma A 2023 *Phys. Rev. A* **107** 043706
[33] Garbe L, Egusquiza I L, Solano E, Ciuti C, Coudreau T, Milman P, and Felicetti S 2017 *Phys. Rev. A* **95** 053854
[34] Deguchi T and Ghosh P K 2009 *Phys. Rev. E* **80** 021107
[35] Chiacchio E I R, Nunnenkamp A, and Brunelli M 2023 *Phys. Rev. Lett.* **131** 113602
[36] Lu X, Li H, Shi J K, Fan L B, Mangazeev V, Li Z M, and Batchelor M T 2023 *Phys. Rev. A* **108** 053712
[37] Li J, Wang Y C, Duan L W, and Chen Q H 2025 *Adv. Quantum Technol.* **8** 2400609
[38] Mandal I and Bergholtz E J 2021 *Phys. Rev. Lett.* **127** 186601
[39] Hodaei H, Hassan A U, Wittek S, Garcia-Gracia H, El-Ganainy R, Christodoulides D N, and Khajavikhan M 2017 *Nature* **548** 187
[40] Fan M S, Zhang H, Shan X L, Yang M L, Yao Y, Lin W, and Liu B 2024 *Opt. Laser Technol.* **172** 110434
[41] Holstein T and Primakoff H 1940 *Phys. Rev.* **58** 1098
[42] Ding K, Ma G C, Xiao M, Zhang Z Q, and Chan C T 2016 *Phys. Rev. X* **6** 021007
[43] Heiss W D and Harney H L 2001 *Eur. Phys. J. D* **17** 149

[44] Zhu K J, Guo Z W, and Chen H 2022 *Acta Phys. Sin.* **71** 131101 (in Chinese)

[45] Manzano D 2020 *AIP Adv.* **10** 025106

[46] Daley A J 2014 *Adv. Phys.* **63** 77

[47] Naghiloo M, Abbasi M, Joglekar Y N, and Murch K W 2019 *Nat. Phys.* **15** 1232

[48] Mi X Y, Liu Y C, Deng Z J, Wu C W, and Chen P X 2025 arXiv:2506.17710 [quant-ph]

[49] Mittal S, Orre V V, Zhu G Y, Gorlach M A, Poddubny A, and Hafezi M 2019 *Nat. Photon.* **13** 692

[50] Hu B, Zhang Z, Zhang H, Zheng L, Xiong W, Yue Z, Wang X, Xu J, Cheng Y, Liu X, and Christensen J 2021 *Nature* **597** 655

[51] Cai H and Wang D W 2021 *Nat. Sci. Rev.* **8** nwaa196

[52] Deng J, Dong H, Zhang C, Wu Y, Yuan J, Zhu X, Jin F, Li H, Wang Z, Cai H, Song C, Wang H, You J Q, and Wang D W 2022 *Science* **378** 966

[53] Wang D W, Song C, Feng W, Cai H, Xu D, Deng H, Li H, Zheng D, Zhu X, Wang H, Zhu S, and Scully M O 2019 *Nat. Phys.* **15** 382

[54] Xu Y and Pu H 2019 *Phys. Rev. Lett.* **122** 193201

[55] Dimer F, Estienne B, Parkins A S, and Carmichael H J 2007 *Phys. Rev. A* **75** 013804

[56] Exner P 2011 Open quantum systems and Feynman integrals (Springer Dordrecht)

[57] Jauho A P and Haug H 2008 *Quantum Kinetics in Transport and Optics of Semiconductors* (Springer Berlin, Heidelberg)

[58] Wu M W, Jiang J H, and Weng M Q 2010 *Phys. Rep.* **493** 61